Check for updates

Received: 26 July 2024 | Revised: 10 December 2024 | Accepted: 12 December 2024

DOI: 10.1002/pro.70012

RESEARCH ARTICLE

THE PROTEIN SOCIETY WILEY

# A functional helix shuffled variant of the B domain of *Staphylococcus aureus*

**Hanna Bobolowski**[1] | **Erik Fiedler**[1] | **Ulrich Haupts**[1] | **Hauke Lilie**[2] | **Ulrich Weininger**[3]

[1]Navigo Proteins GmbH, Halle, Germany

[2]Department of Biotechnology and Biochemistry, Martin-Luther-University Halle-Wittenberg, Halle, Germany

[3]Institute of Physics, Biophysics, Martin-Luther-University Halle-Wittenberg, Halle (Saale), Germany

**Correspondence**
Ulrich Weininger, Institute of Physics, Biophysics, Martin-Luther-University Halle-Wittenberg, Halle (Saale), Germany.
Email: ulrich.weininger@physik.uni-halle.de

**Review Editor:** Lynn Kamerlin

**Abstract**

The B domain of protein A is a biotechnologically important three-helix bundle protein. It binds the Fc fragment of antibodies with helix 1/2 and the Fab region with helix 2/3. Here we designed a helix shuffled variant by changing the connectivity of the helices, in order to redesign the helix bundle, yielding altered helix–loop–helix properties. The new loops that generate the new connectivity were created in several protein libraries, and Fc binding variants were selected for a detailed biochemical characterization. We were able to create variants with Fc binding affinity at the same level as the wild type B but with significantly reduced thermal stability. The NMR structure proved that the overall three-dimensional structure was maintained not only in the helix shuffled variant but also points to some potential local differences to wild-type B, which could be the reason for the reduced thermal stability. Therefore, protein A is an example of an optimized structure being more important for stability than for function. Using the helix shuffled variant as a ligand on an affinity column facilitates a robust and straightforward purification of antibodies, but allows for a milder elution at less extreme pH. Therefore, the helix shuffled variant is a suitable ligand to purify more pH-sensitive antibodies.

**KEYWORDS**

NMR spectroscopy, protein A, protein binding, protein engineering, ribosome display

## 1 | INTRODUCTION

Proteins fulfill a large number of important biological functions in cells. They provide structure to parts of the cells, ensure movements within the cell, and are responsible for enzymatic catalysis, specific binding, and regulation (Litwack, 2017). Their specific functions are directly linked to their three-dimensional structures (Fersht, 1977). In the case of specific recognition and binding, one of the main functions of proteins, the involved amino acid side chains are arranged in the required structural context, e.g., hormones must bind to their receptors to exert their effects, other proteins bind to proteins to determine their translocation or to mark them for degradation. After binding, proteins can change the bound molecule, adjust their own structural conformation, or even trigger subsequent reactions by encountering a third molecule (Boehr et al., 2006; Köhler et al., 2020).

Protein A (PrA) is a structurally well-characterized (Deisenhofer, 1981) 42 kDa multidomain surface protein

This is an open access article under the terms of the Creative Commons Attribution-NonCommercial License, which permits use, distribution and reproduction in any medium, provided the original work is properly cited and is not used for commercial purposes.
© 2025 The Author(s). *Protein Science* published by Wiley Periodicals LLC on behalf of The Protein Society.

located in the cell wall of *Staphylococcus aureus*. Its five immunoglobulin G (IgG) binding domains (E, D, A, B, and C) each display a three-helix bundle topology and a sequence identity between 74% and 91% compared to domain A. Each domain folds independently by apparent two-state folding (Myers & Oas, 2001) and displays high thermal and chemical stability against unfolding. The proteins unfold at a temperature of ~70°C and are resistant to treatment with acidic solutions (pH 3.0) (Rigi et al., 2019). PrA and variants thereof are the most prominent affinity ligands in antibody purification ranging back to 1978 (Ey et al., 1978). The 6.6 kDa B domain of PrA served as a template for the development of artificial or synthetic binding domains, like synthetic Z domain with high stability under alkaline pH conditions (Linhult et al., 2004). Its tertiary structure is characterized by three amphipathic helices with antiparallel orientation connected by two highly conserved loops that form a small bundle (Figure 1a). The three-helix bundle is stabilized by a variety of noncovalent interactions in the α-helical regions of the protein, but also between loops and helices (Shao & Gao, 2011).

The B domain binds with its N-terminal two helices to the hinge region between the CH2 and CH3 domains of the Fc region of antibodies (Deisenhofer, 1981). Upon Fc binding, the helices 1 and 2 undergo conformational changes regarding their relative orientation. The key residues of Fc binding in the B domain are F5, Q9, Q10, N11, F13, Y14, L17 (helix 1) and N28, I31, Q32, K35 (helix 2), which have been confirmed by mutant analysis and x-ray crystallography (Deis et al., 2015). Furthermore, a construct only consisting of the N-terminal two helices binds Fc with similar affinity but shows less thermodynamic stability (Starovasnik et al., 1997). Like all Protein A domains, the B domain also binds the Fab region of antibodies via the helix 2/3 interface (Graille et al., 2000). Again, these helices reorient towards each other upon binding. Key residues for Fab binding are Q26, G29, F30, Q32, S33, D36 (helix 2) and N43, E47, L51 (helix 3). The binding affinity to Fab is about 30-fold weaker compared to Fc binding. Beyond the specific binding to Fc and Fab fragments of antibodies, PrA was used as a scaffold for the generation of engineered binding proteins (Fiedler et al., 2022; Gebauer & Skerra, 2020; Kahl et al., 2021; Ståhl et al., 2017).

In the last decades, PrA has been a prominent candidate for protein engineering. In fact, helical proteins have a rich history in design and redesign. Starting historically with the design of soluble isolated helices (Shoemaker et al., 1985), followed by the design of four-helix bundle proteins including helix sequence, helix contacts, and loop sequences (Degrado et al., 1989; Richardson & Richardson, 1988). Nowadays, protein engineering, in combination with synthetic libraries and various selection systems, has enabled the design of artificial binding proteins with desired properties. Thus, more than 50 so-called alternative scaffold proteins have been described (Garg, 2021). These scaffolds form an extremely divergent group of binding proteins that differ in their origin, size, and structural topology. Due to their small size and simplified manufacturability compared to antibodies, these binding proteins offer advantages in therapy and diagnostics and are suitable as ligands for chromatographic applications (Gebauer & Skerra, 2020). First attempts on switching helix connections were made with four-helix bundle proteins such as ROP (Kresse et al., 2001; Predki & Regan, 1995). These studies showed that it is possible to rearrange the helices by inserting loops. However, the length and composition of the loops were a crucial factor for the stability of the bundle. For three-helix bundles domain Z, grafting of loops (Kanje et al., 2020) and target residues (Gunneriusson et al., 1999) onto

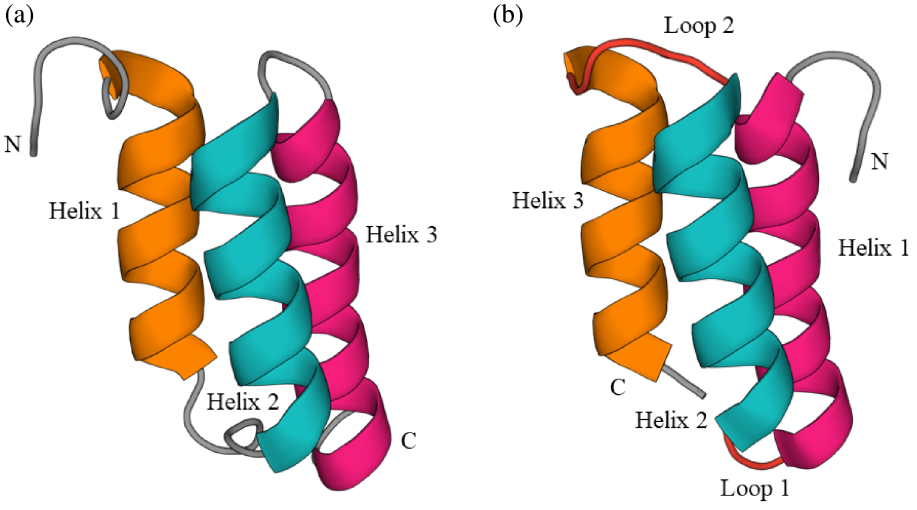


**FIGURE 1** Helix shuffling strategy for the generation of functional domain B variants. (a) Structural elements of wild type domain B in their original order. Starting from the N-terminus (N), the three helices are colored orange (helix 1), cyan (helix 2), and pink (helix 3). Helix connecting loops are colored gray. (b) Applied helix shuffling strategy based on domain B. Compared to wild type, the order of the helices 1 and 3 is swapped. Alternative loops (red) with several randomized positions are inserted to form a three-helix bundle and generate diversity.

1469896x, 2025, 2, Downloaded from https://onlinelibrary.wiley.com/doi/10.1002/pro.70012, Wiley Online Library on [22/01/2025]. See the Terms and Conditions (https://onlinelibrary.wiley.com/terms-and-conditions) on Wiley Online Library for rules of use; OA articles are governed by the applicable Creative Commons License

existing structural elements was used to design proteins with altered function and stability. In addition, de novo design of thermostable helix bundles with different connectivity of structural elements was conducted (Huang et al., 2014).

In this work, we generated helix shuffled variants of domain B that are suitable as affinity ligands, the first time such an approach was applied for three-helix bundle proteins. We kept the natural three helices, including all the key residues of binding, but connected them differently with two alternative loops possessing several randomized positions (Figure 1b), potentially affecting the conformational changes of the helices upon target binding. NMR structure determination proved that the helix shuffled variant possesses the expected overall three-dimensional structure, although with some potential local differences compared to wild-type (wt) domain B. This might explain a reduced thermodynamic stability. However, the binding affinity to Fc is at the same level as the wt. Taken together, we show a successful helix-shuffled variant for domain B of protein A in particular and for a three-helix bundle protein in general. This redesigned domain opens the way to address the binding of antibodies and other possible targets. Hereby the changed helix loop dynamics and stability of the new domain provide new approaches and application strategies within the protein A field.

## 2 | RESULTS & DISCUSSION

In order to successfully create a helix shuffled variant of the B domain, we first investigated the influence of loops on structure and function. For this, the loops were partially or completely replaced by glycine and serine residues displaying high conformational freedom (van Rosmalen et al., 2017). Variants generated with this rational engineering approach showed a lower affinity for Fc (Table S1) and to some extent a lower proportion of α-helical structures (50%–60%) compared to wild-type domain B (~70%) (Table S2), especially when modifying loop 1. Nevertheless, these results showed that both loops of domain B can be substituted to a certain extent, without destroying the functionality and structure of the protein.

In the next step, the logical position of the helices in the three-helix bundle was swapped by helix shuffling with respect to the primary sequence. However, their orientation within the 3D structure remained the same (Figure 1b). Loop lengths were chosen from databases and initial MD simulations but varied in the selection process. Initial AlphaFold models suggest that such variants should be folded and look like the wt (with different loops). Consequently, two alternative loops with several randomized positions (excluding C, W, H, Y, and F) were inserted to connect the rearranged structural elements and generate diversity. A loop length of three to five (loop 1) and six to eight (loop 2) residues was selected to cover the calculated interhelical distances (Figure S1). Altogether, four libraries with 9–12 randomized positions and diversities of $1.8 \times 10^{10}$–$1.7 \times 10^{12}$ were generated. Hence, the length of the novel loops was comparable to loops found in other helix bundle proteins, mostly consisting of up to 15 residues (Choi et al., 2013). Libraries with comparable theoretical diversity were mixed in equal proportions and named (3/6), (3/7_4/6), (3/8_4/7_5/6), and (4/8_5/7), indicating the number of residues in loop 1/loop 2 (Table S3).

### 2.1 | Screening of helix shuffled domain B variants

IgG-binding variants were selected by ribosome display followed by an automated high-throughput (HTS) ELISA-based screening. In order to cover a hit rate of 1%, 12,960 variants were screened with a comparable scope of 3240 variants per library. A total of 2666 variants, so-called hits, showed an IgG-binding signal ≥3× standard deviation of the mean of the negative control (empty expression vector) and were selected for secondary screening. Hence, hit rates between 20% and 22% were achieved for the libraries (3/7_4/6), (3/8_4/7_5/6) and (4/8_5/7). A clearly reduced hit rate was observed for the library (3/6) indicating that loop 1 with a length of three and loop 2 with six residues might be too short. Therefore, significantly longer loops, as found in the remaining three libraries with four or five (loop 1) and seven or eight residues (loop 2), are probably better suited to form functional helix bundles. Based on protein expression and absolute amplitude of the IgG binding signal, 461 hits were selected for precise functional characterization. For this screening, binding to Fc was investigated by biolayer interferometry (BLI). As a result, 424 variants showed high-affinity binding to hIgG1-Fc, whereas BSA as a negative control was not bound. One hundred and forty-seven variants possessing the highest affinity for hIgG1-Fc compared to the others were selected for tag-free production and re-determination of IgG-binding by surface plasmon resonance (SPR). Except five all variants showed binding to hIgG1-Fc with different kinetic parameters $k_{on}$ and $k_{off}$. The dissociation rates of the variants were significantly increased by at least factor 15 compared to wild-type domain B, whereas $k_{on}$ was only slightly affected by a factor of 2, showing that the lower affinity arises from a shorter lifetime of the complex

1469896x, 2025, 2, Downloaded from https://onlinelibrary.wiley.com/doi/10.1002/pro.70012, Wiley Online Library on [22/01/2025]. See the Terms and Conditions (https://onlinelibrary.wiley.com/terms-and-conditions) on Wiley Online Library for rules of use; OA articles are governed by the applicable Creative Commons License

**TABLE 1** Parameters of the binding of domain B variants to hIgG1.[a]

| Loop 1/loop 2 | $k_{on}$ ($M^{-1}$ $s^{-1}$) | $k_{off}$ ($s^{-1}$) | $K_D$ (M) |
|---|---|---|---|
| LPNL/DPSQ (wt) | $7.6 \times 10^5$ | $0.6 \times 10^{-2}$ | $0.1 \times 10^{-7}$ |
| GGIT/AKTNPGN | $6.5 \times 10^5$ | $2.4 \times 10^{-2}$ | $0.4 \times 10^{-7}$ |
| GGLT/VRKLGP | $4.7 \times 10^5$ | $2.2 \times 10^{-2}$ | $0.5 \times 10^{-7}$ |
| NGLT/VRTNGA | $6.1 \times 10^5$ | $2.3 \times 10^{-2}$ | $0.4 \times 10^{-7}$ |
| GGLT/VRRVGS | $2.2 \times 10^5$ | $6.0 \times 10^{-2}$ | $2.7 \times 10^{-7}$ |
| GGLT/GTEGVH | $1.7 \times 10^5$ | $6.1 \times 10^{-2}$ | $3.6 \times 10^{-7}$ |
| GGLT/NRLTKD | $0.5 \times 10^5$ | $2.2 \times 10^{-2}$ | $4.2 \times 10^{-7}$ |
| GGIT/AKRNPMT | $2.2 \times 10^5$ | $1.1 \times 10^{-2}$ | $5.1 \times 10^{-7}$ |
| GGLT/MNVGKH | $4.2 \times 10^5$ | $4.1 \times 10^{-2}$ | $7.8 \times 10^{-7}$ |
| GGLT/ASEKGA | $1.1 \times 10^5$ | $7.9 \times 10^{-2}$ | $7.9 \times 10^{-7}$ |
| GGLT/TAANPTA | $2.1 \times 10^5$ | $17 \times 10^{-2}$ | $8.2 \times 10^{-7}$ |
| GGIT/AKANPEA | $0.4 \times 10^5$ | $4.4 \times 10^{-2}$ | $11.8 \times 10^{-7}$ |
| GGLT/PVLRGKP | $1.9 \times 10^5$ | $25 \times 10^{-2}$ | $12.8 \times 10^{-7}$ |
| GGIT/ALRGHD | $1.5 \times 10^5$ | $23 \times 10^{-2}$ | $15.6 \times 10^{-7}$ |
| GGLT/HTPTRG | $0.2 \times 10^5$ | $13 \times 10^{-2}$ | $64.2 \times 10^{-7}$ |

[a]$k_{on}$ is an association rate constant. $k_{on}$ is a dissociation rate constant. $K_D$ is an equilibrium dissociation constant and the ratio between $k_{off}$ and $k_{on}$.

**TABLE 2** Calculated α-helical structures and $T_m$ values of domain B variants.

| Loop 1/loop 2 | Helix (%) | $T_m$ (°C) |
|---|---|---|
| LPNL/DPSQ (wt) | 72.1 ± 5.1 | 71.0 ± 1.3 |
| GGIT/AKTNPGN | 72.0 ± 3.2 | 31.2 ± 1.0 |
| GGLT/VRKLGP | 71.2 ± 3.5 | 29.5 ± 0.7 |
| NGLT/VRTNGA | 71.9 ± 1.2 | 32.4 ± 0.6 |
| GGLT/VRRVGS | 71.2 ± 7.2 | 32.8 ± 1.8 |
| GGLT/GTEGVH | 63.7 ± 6.9 | 28.1 ± 0.3 |
| GGLT/NRLTKD | 70.6 ± 7.8 | 31.6 ± 2.1 |
| GGIT/AKRNPMT | 71.3 ± 5.2 | 32.4 ± 1.8 |
| GGLT/MNVGKH | 70.8 ± 2.1 | 31.0 ± 0.5 |
| GGLT/ASEKGA | 70.9 ± 2.6 | 30.8 ± 1.2 |
| GGLT/TAANPTA | 68.7 ± 8.8 | 30.7 ± 0.9 |
| GGIT/AKANPEA | 67.9 ± 7.3 | 31.5 ± 2.3 |
| GGLT/PVLRGKP | 70.3 ± 7.2 | 29.7 ± 1.8 |
| GGIT/ALRGHD | 68.7 ± 4.9 | 30.6 ± 2.9 |
| GGLT/HTPTRG | 56.5 ± 6.0 | 31.1 ± 2.1 |

(Figure S2). This indicates that the variants exist in a ready to bind conformation, but contacts in the bound form provide less stability, hence they dissociate faster. At the end of the screening, 24 IgG-binding variants with the highest affinity compared to the others were selected for sequence analysis and detailed biochemical characterization.

## 2.2 | Loop composition of helix shuffled domain B variants

After selection, the obtained pools of IgG-binding domain B variants were analyzed by next-generation sequencing (NGS, Eurofins) resulting in more than 1,200,000 sequences. Significant differences in the amino acid distribution within the randomized loops were observed compared to the initial libraries, indicating a successfully applied selection pressure during ribosome display. In general, the analyzed variants showed high diversity in the randomized loops (Tables 1 and 2, Figure S3). In loop 1, connecting the helices 1 and 2, the present motif (GGI/LT) predominated. Small and highly flexible glycine are frequently found in loops, because they accelerate loop formation by decreasing the activation energy and are postulated to play an important role in chain compaction during the early stages of folding (Krieger et al., 2005). Threonine, which frequently forms hydrogen bonds in loops (Worth & Blundell, 2010), might form additional interactions with the helices 1 and 2 thus stabilizing the helix 1/2 arrangement. Hydrophobic leucine/isoleucine, an original loop residue of domain B involved in the formation of noncovalent interactions, could also contribute to the stabilization of the alternative scaffold. Compared to loop 1, higher diversity was observed in loop 2 that connects the helices 2&3. However, accumulations of certain amino acids at individual positions were detected. Possibly, loop 2 has a high degree of structural flexibility without significantly affecting the formation of

1469896x, 2025, 2, Downloaded from https://onlinelibrary.wiley.com/doi/10.1002/pro.70012, Wiley Online Library on [22/01/2025]. See the Terms and Conditions (https://onlinelibrary.wiley.com/terms-and-conditions) on Wiley Online Library for rules of use; OA articles are governed by the applicable Creative Commons License

the helix 2/3 interface and thus folding of the protein. Thus, the obtained loop length corresponds well to loops found in other three- and four-helix bundle proteins such as ABD (Nilvebrant & Hober, 2013) and cytochrome c (Dobbs et al., 1996).

The sequence analysis of the 24 IgG-binding variants obtained after the screening process revealed similar trends in terms of loop length and composition (Figure S3). Four of the examined variants contained a shifted reading frame at DNA level (4×) and were not used for further experiments. From the remaining 20 variants, 13 were obtained from the libraries (3/7_4/6) and 7 from (3/8_4/7_5/6), underlining the favorable loop design constrictions of these. In summary, it can be assumed that the enriched motif (GGI/LT) and the defined length of the loops are directly related to the functionality (IgG binding) of these variants.

## 2.3 | Functional analysis of helix shuffled domain B variants

From the remaining 20 domain B variants, 14 variants could be produced and used for functional and structural characterization. Four variants showed mainly insoluble expression and another 2 variants completely precipitated during purification. Firstly, purified variants were analyzed in detail by SPR regarding their affinity for hIgG1-Fc. All variants showed binding to hIgG1-Fc with affinities ranging from $K_D = 10^{-6}$–$10^{-8}$ M (Figure 2, Table 1). The best binders were on the level of the wt domain ($K_D = 1 \times 10^{-8}$ M) and slightly outperformed the construct of only the two Fc binding helices ($K_D = 1.8 \times 10^{-7}$ M) (Starovasnik et al., 1997). Weaker binding arose from an increase in dissociation rate constant $k_{off}$, whereas $k_{on}$ was less affected. Even for variants that showed a lower affinity compared to wt, the obtained $K_D$ values are in line with typical affinities of other engineered binding proteins (Mouratou et al., 2015), antibodies, or antibody fragments (Kikuchi et al., 2005).

Next, the affinity of variants for the Fab fragment was analyzed. The Fab-fragment of Avelumab, an FDA-approved PD-L1 antibody, was used as a representative target. The variants showed no binding to Avelumab-Fab, whereas the affinity of wt B for the target was confirmed (Figure S4, Table S4). This was expected, because our strategy in creating functional domain B variants focused on Fc-binding and the helix 1/2 interface, rather than the helix 2/3 interface that mediates binding to the Fab fragment. All taken together, we were successful in creating and selecting functional helix shuffled domain B variants with high binding affinity to hIgG1-Fc.

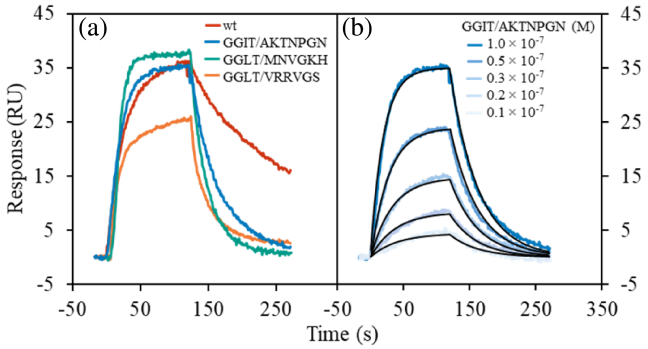


**FIGURE 2** Determination of the dissociation constants of IgG-binding domain B variants. (a) Binding of three domain B variants with different loop 1/loop 2 composition to hIgG1-Fc. Wild type (wt) domain B is shown as a comparison. hIgG1-Fc was immobilized on the surface of a CM5 chip using NHS chemistry. Binding of variants at a concentration of, $1.0 \times 10^{-7}$ M to hIgG1-Fc was determined at a flow rate of 30 μL/min. 1x PBST 0.05% (v/v) pH 7.3 was used as a running buffer. (b) Binding of one variant with (GGIT/AKTNPGN) loops at different concentrations to immobilize hIgG1-Fc. Association ($k_{on}$) and dissociation ($k_{off}$) rates were determined using a Langmuir fitting model. $K_D$ is an equilibrium dissociation constant and the ratio between $k_{off}$ and $k_{on}$.

## 2.4 | Helical content and stability analysis of helix shuffled domain B variants

Furthermore, the secondary structure and the thermal stability of the variants were investigated by CD. Except two all variants showed a CD spectrum and a calculated α-helical proportion (~70%) comparable to wild-type domain B (Figure 3, Table 2), indicating that the helices remain folded after helix shuffling. Next, temperature-induced unfolding and refolding of domain B variants were measured to investigate the thermal stability of the proteins. A significant decrease in $T_m$ was detected for all the novel domain B variants ($T_m \sim 30°C$) compared to wt domain B ($T_m = 72.1°C$). The construct of only the two Fc binding helices displayed an even further reduced $T_M$ (~10°C) (Starovasnik et al., 1997). These finding is in line with an engineering approach by Gülich et al. in which the natural loops of domain Z were replaced or extended by glycines to decrease the thermal stability making a less stable protein (Gülich et al., 2000). This shows, that while the helices are folded, their packing to a three-helix bundle is less strong in all helix-shuffled variants. The natural loops of domain B contribute to folding and stability by forming a variety of noncovalent interactions between highly conserved amino acids in loops and the helices (Shao & Gao, 2011), which might be missing in the helix shuffled variant. Fc binding affinity and stability are not correlated and have to be addressed independently in the

1469896x, 2025, 2, Downloaded from https://onlinelibrary.wiley.com/doi/10.1002/pro.70012, Wiley Online Library on [22/01/2025]. See the Terms and Conditions (https://onlinelibrary.wiley.com/terms-and-conditions) on Wiley Online Library for rules of use; OA articles are governed by the applicable Creative Commons License

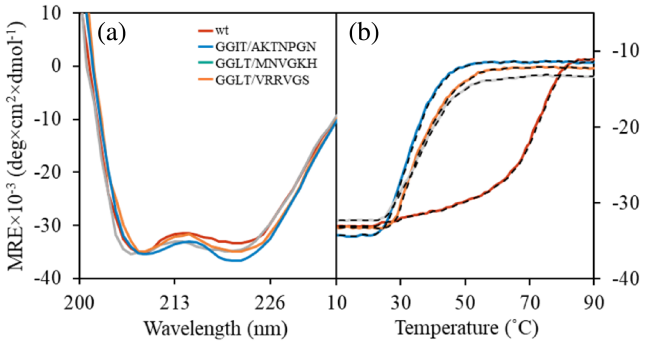


**FIGURE 3** Circular Dichroism spectra and thermal-induced structural transition of domain B variants. (a) The mean residue ellipticity (MRE) is calculated based on the CD signals in the far UV region. Wild-type domain B (wt) is shown as a comparison. The CD measurements were performed at room temperature with a protein concentration of 0.2 mg/mL in 20 mM $NaH_2PO_4$pH 7.3. (b) Thermal-induced structural transition of domain B variants was measured at a wavelength of 222 nm. The melting temperature ($T_m$) was calculated using a sigmoidal 4-parameter fit (black dashed lines).

design of the three-helix bundle. In the first approach presented here, we selected primarily Fc binding without addressing stability simultaneously. For technical reasons, the selection was performed at 15°C to allow the formation of temperature-sensitive ternary complexes during ribosome display. To enrich proteins with an increased thermal stability, more robust selection methods such as phage (Pershad & Kay, 2013) and mRNA display (Wang & Liu, 2011) could be used.

## 2.5 | 3D structure determination of the helix shuffled domain B

The novel domain B variant (GGIT/AKTNPGN) was selected for 3D structure determination because the protein showed the best manufacturability, the highest affinity for hIgG1-Fc, and a domain B-like proportion of α-helical structures compared to the other variants. NMR spectroscopy was used to determine the 3D structure of (GGIT/AKTNPGN) and to localize Fc binding sites on the surface of the protein. About 90% of the amide signals (proline excluded) in the $^{1}H^{15}N$-HSQC could be assigned by HNCA(CO)CB/HNCACB experiments. This is somewhat less than typical assignment levels of 95% and above, caused by the limited spectral dispersion (Figure S5), and possibly increased amide exchange in the artificially designed protein. Resonances from side chains in the $^{1}H^{13}C$-HSCQs have been assigned by $^{15}N$-TOCSY-HSQC and HCCH-TOCSY experiments. Here, 96% of the resonances could be assigned. This is a typical assignment level for well-behaving proteins and confirms the suspected problem of enhanced amide exchange for the amide assignment (data not shown).

**TABLE 3** Statistics of the NMR structure determination.

| **NMR distance and dihedral constraints** | |
|---|---|
| Total NOE | 429 |
| Intraresidue | 202 |
| Sequential ($\|i–j\| = 1$) | 81 |
| Medium ($\|i–j\| < 4$) | 87 |
| Long ($\|i–j\| > 5$) | 59 |
| Phi | 39 |
| Psi | 39 |
| *Violations (mean and SD)* | |
| Distance constraints, Å | 0.03 ± 0.01 |
| Dihedral angle constraints, ° | 0.8 ± 0.2 |
| *Ramachandran analysis* | |
| Most favored, % | 84.7 |
| Additionally allowed, % | 11.6 |
| Generously allowed, % | 1.8 |
| Disallowed, % | 1.8 |
| *Deviations from idealized geometry* | |
| Bonds lengths, Å | 0.003 |
| Bond angles, ° | 0.47 |
| Impropers, ° | 1.24 |
| *Average pairwise rmsd, Å* | |
| Heavy, all | 2.8 ± 0.4 |
| Backbone, all | 2.2 ± 0.4 |
| Heavy, 2nd structure | 1.4 ± 0.2 |
| Backbone, 2nd structure | 0.8 ± 0.2 |

A total of 429 unique NOEs and 78 TALOS+ derived phi/psi restraints could be used for the final structure calculation. The number of NOEs is less than can be usually used in NMR structure calculations of proteins of similar sizes. This is again caused by a reduced spectral dispersion. Therefore, the final structural ensemble displays a reduced precision. The overall structural statistics (Table 3) are all in all decent, but sometimes slightly below reference statistics, as expected from the reduced number of unique NOEs. The structural ensemble shows the expected three-helix bundle (Figures 4 and S6). Helix 1 (3 in wt) the first loop and the majority of helix 2 display a high-precision structural region. However, the length of helix 2 is reduced C-terminally. Furthermore, the second loop is structurally undefined and consequently the attachment of helix 3 (1 in wt) appears to be less defined. All in all, the structure not only proves the expected overall geometry but also highlights the problematic part, the second loop with the directly connected parts of helix 2 and helix 3 (1 in wt).

1469896x, 2025, 2, Downloaded from https://onlinelibrary.wiley.com/doi/10.1002/pro.70012, Wiley Online Library on [22/01/2025]. See the Terms and Conditions (https://onlinelibrary.wiley.com/terms-and-conditions) on Wiley Online Library for rules of use; OA articles are governed by the applicable Creative Commons License

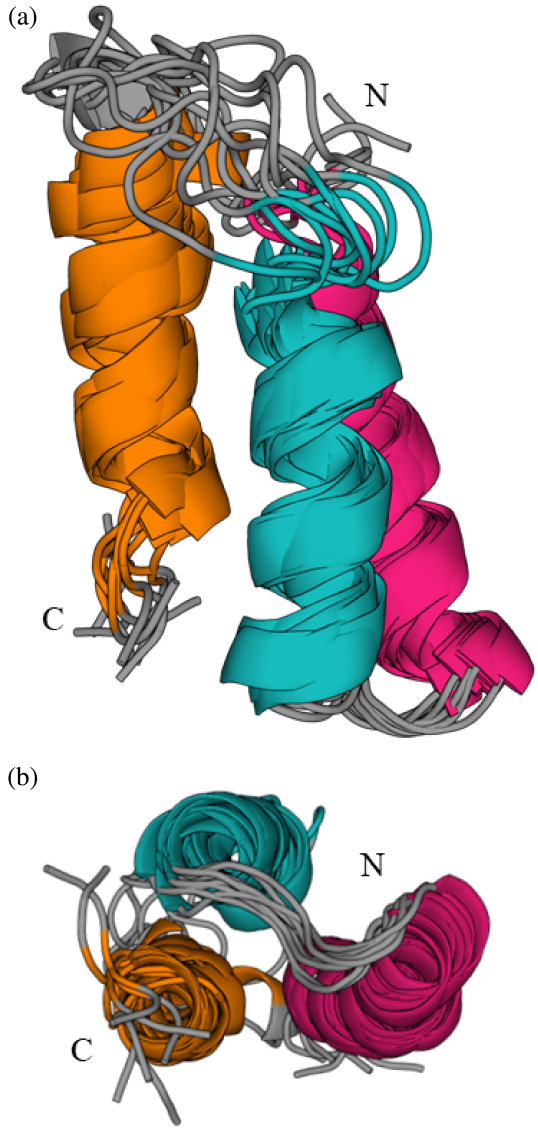


**FIGURE 4** 3D structure determination of the helix shuffled domain B variants (GGIT/AKTNPGN). (a) Overlay of 10 NMR structures of (GGIT/AKTNPGN). Starting from the N-terminus the three helices are colored pink (helix 1), cyan (helix 2), and orange (helix 3). The helix connecting loops and the termini are colored gray. (b) Alignment of helix shuffled domain B compared to wild type as top view.

## 2.6 | Fc binding site

An NMR titration experiment with hIgG1-Fc as a binding partner was performed to identify the Fc binding site. In four steps, unlabeled hIgG1-Fc ($c = 0$, 30, 70, 130 μM) was titrated to the $^{13}C^{15}N$ labeled helix shuffled variant ($c = 91$ μM). The corresponding $^{1}H^{15}N$-TROSY-HSQC spectra showed a decrease in intensity but no observable shift of the NMR signals (Figure S7), indicative of the slow NMR exchange regime and a long lifetime of the formed complex. The decrease in signal intensity affected almost all signals either directly, by changing the chemical shift from the free to the bound state (which is not observable because of the large size of the complex), or indirectly by increased relaxation losses in the much bigger complex. These two effects can be distinguished by a higher order of reduced intensity in the case of direct binding (here the intensity must decrease to zero in case of a fully formed complex, because the signals of the bound state would appear somewhere else if they would be observable) and a lower order of reduced intensity in case of indirectly increased relaxation (here the intensity will decrease to a certain value in case of a fully formed complex). These two cases were distinguished under substoichiometric conditions, in which the signals display still a reasonable intensity. The obtained volumes of the integrated peak areas were normalized to the values of free $^{13}C^{15}N$ protein. The NMR signals of I25, I34, Q35, K38, Q51, F55, Y56, and L59 changed significantly (plot signal ≤50%) upon binding of hIgG1-Fc. T26, N31, and N53 displayed a loss of peak volume between 35% and 50%, while others either were unaffected or did not give clear results (Figures 5 and S6). All in all, the Fc binding site of the helix shuffled variant identified by NMR titration is in very good agreement with the known Fc binding site of the wt. Small differences can be caused by the mapping of the binding site by backbone amides and not by the directly involved side chains. Additionally, the overlap in Fc binding epitopes of (GGIT/AKTNPGN) and wild-type B was demonstrated by a competitive ELISA (Figure S8). The whole binding site is located in the well-folded region of the helix shuffled variant on helix 2 and 3. The shortening of helix 2 and the disordered loop 2 is not involved in binding, explaining why the region of structural problems does not affect the binding strength. However, they still enable the conformational dynamic of the two helices needed for Fc binding. In addition to the binding, site residues I25 and T26 in loop 1 display differences upon binding. Because they are not in the known binding site, they likely point to conformational changes of $^{13}C^{15}N$ domain B variant (GGIT/AKTNPGN) during complex formation, mediated by loop 1. Binding between proteins is usually associated with structural rearrangements, ranging from small local changes in the side chains (lock-and-key) to global changes in the entire tertiary structure (induced-fit) (Tobi & Bahar, 2005). Such conformational changes upon Fc binding have also been described for domain B and its engineered descendant domain Z. Deis et al. observed a decrease in conformational heterogeneity upon Fc binding and a side chain substitution of domain B for an Fc side chain adjusted to the binding surface (Deis et al., 2015). These findings could explain the slightly different side chain orientations of the identified residues of

1469896x, 2025, 2, Downloaded from https://onlinelibrary.wiley.com/doi/10.1002/pro.70012, Wiley Online Library on [22/01/2025]. See the Terms and Conditions (https://onlinelibrary.wiley.com/terms-and-conditions) on Wiley Online Library for rules of use; OA articles are governed by the applicable Creative Commons License

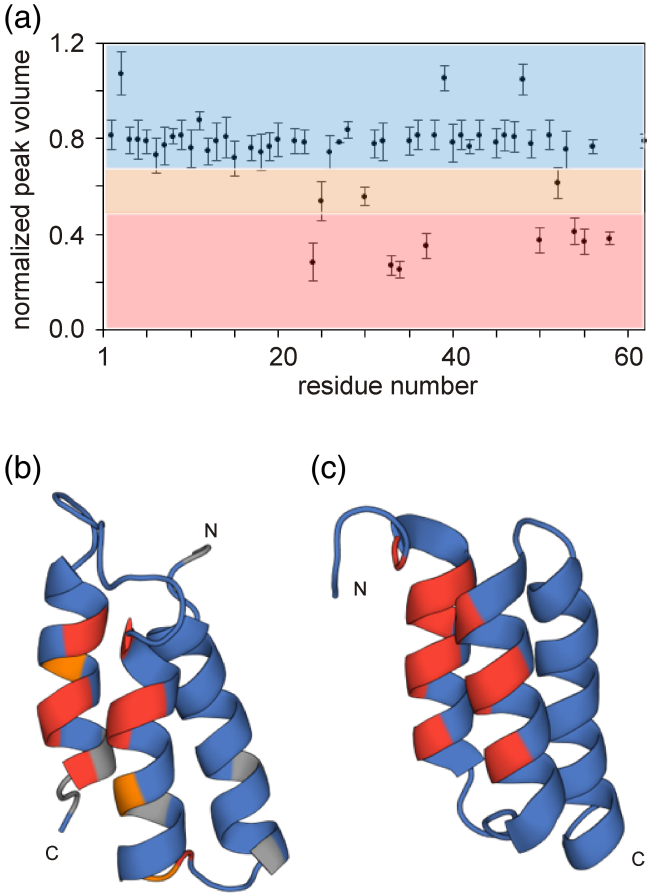


**FIGURE 5** Fc binding sites of helix shuffled domain B and wildtype. (a) An NMR titration experiment was performed to identify the Fc binding site of domain B variant (GGIT/AKTNPGN). Integrated peak areas (intensities) obtained from the $^{1}H^{15}N$-TROSY-HSQC spectra of the 1:0.35 complex (domain B:Fc) were normalized to the spectrum of free $^{13}C^{15}N$ domain B. Red colored residues (I25, I34, Q35, K38, Q51, F55, Y56, and L59) showed a significant decrease in NMR peak volume (≤0.5) upon Fc binding. Orange-colored residues (T26, N31, and N53) lost between 30% and 50% (≤0.70) of their NMR peak volume. Blue-colored residues showed no changes in the backbone NMR signal. (b) Mapping of Fc binding sites of (GGIT/AKTNPGN) identified by the NMR titration experiment on the 3D structure. (c) Natural Fc binding sites (red) of wild-type domain B are located on helices 1 and 2.

domain B variant (GGIT/AKTNPGN) probably involved in Fc binding. Due to the conformationally heterogeneous nature of individual Protein A domains, exact side chain orientations are only transferrable to a very limited extent to those of domain B variant (GGIT/AKTNPGN). In contrast, some conformational restriction, mediated by the additional helix, which is not directly involved in binding, seems to be of benefit, because the helix shuffled variant binds to Fc with higher affinity ($0.4 \times 10^{-7}$ M) than a construct of only the two Fc binding helices ($1.8 \times 10^{-7}$ M). From a structural view, it is unclear why the Fab binding capability was lost, because all key residues for Fab binding are in the structurally unaltered and well-defined part of the helix shuffled variant (helices 1 & 2). Potentially, some required conformational dynamics among these helices were lost in the optimization of loop 1 for Fc binding only. In summary, the helix shuffled variant binds Fc as the wt, only with slightly reduced affinity (Table 1), arising from higher $k_{off}$, indicating the contacts in the complex provide less stability.

## 2.7 | Domain B variant (GGIT/AKTNPGN) as affinity ligand for the purification of hIgG1

Protein A affinity chromatography is typically used for the purification of antibodies or Fc-fusion proteins. Therefore, the suitability of (GGIT/AKTNPGN) as an affinity ligand was investigated. The helix shuffled variant was coupled to HiTrap NHS-Activated HP resin (Cytiva) and hIgG1 was loaded onto the column followed by an elution with a linear gradient of pH 7.3 to 3.0. By using the (GGIT/AKTNPGN) column, hIgG1 was captured and eluted with high recovery (≥95%) with a peak maximum at pH 4.8. This pH value was significantly higher compared to pH 3.7 from a wt B domain column (Figure S9). These results suggest that (GGIT/AKTNPGN) could be used for milder elution of pH-sensitive antibodies and Fc-fusion proteins (Wang et al., 2024). In other studies, pH-sensitive protein A was produced by introducing histidine mutations (Tsukamoto et al., 2014) and inserting loop extensions (Gülich et al., 2000). Further, the engineered domain $Z_{Ca}$ with an inserted calcium-binding motif inspired by the calmodulin loop enabled mild elution of antibodies (Scheffel et al., 2019). In addition, thermo-sensitive protein A domains such as Bryzen Pro can be mentioned (Krepper et al., 2018).

The dynamic binding capacity (DBC) of the (GGIT/AKTNPGN) column at 10% breakthrough was determined with 18.2 mg/mL (data not shown). This was about 65% of the DBC determined for the resin with coupled wild-type domain B (28.1 mg/mL). For traditional protein A resins, binding capacities of ≥65 mg/mL are described (Ghose et al., 2014). However, these ligands are only partially comparable to (GGIT/AKTNPGN) because these are next-generation tandem repeat proteins. Such tandem repeats in combination with directed coupling of the ligand are useful strategies to significantly increase the binding capacity of the chromatographic column.

Last, purification of hIgG1 spiked in cell culture harvest was performed to test the ability of (GGIT/

1469896x, 2025, 2, Downloaded from https://onlinelibrary.wiley.com/doi/10.1002/pro.70012, Wiley Online Library on [22/01/2025]. See the Terms and Conditions (https://onlinelibrary.wiley.com/terms-and-conditions) on Wiley Online Library for rules of use; OA articles are governed by the applicable Creative Commons License

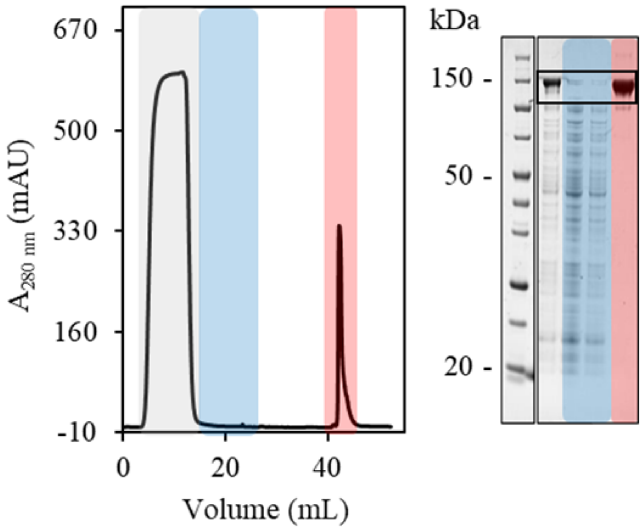


**FIGURE 6** (GGIT/AKTNPGN) as affinity ligand for the purification of hIgG1. Domain B(GGIT/AKTNPGN) was immobilized at 10 mg/mL on HiTrap NHS-Activated HP resin (Cytiva). Clarified Expi293 cell culture harvest spiked with hIgG1 (0.2 mg/mL) was used as load material. After a wash step, bound hIgG1 was eluted in a linear gradient between pH 7.3 and 3.0 (left image). Load (gray), wash (blue), and elution (red) fractions were analyzed by SDS-PAGE (right image).

AKTNPGN) to selectively purify antibodies. As a result, hIgG1 was successfully isolated from the cell culture material with excellent purity (≥95%) and high recovery (≥91%) (Figure 6). Ten cycles of hIgG1 loading and elution were performed to investigate the column lifetime. After each cycle, the column was regenerated using 10 CV 100 mM citrate pH 2.0. As a result, a functionality of 90% was observed for (GGIT/AKTNPGN), whereas no reduction of column performance was detected for wild-type domain B (data not shown). In conclusion, (GGIT/AKTNPGN) offers high potential as an affinity ligand for the purification of antibodies. It effectively captured hIgG1 and allowed for a milder elution at less extreme pH (4.8 instead of <3.7). This enables the purification of more pH-sensitive proteins.

## 2.8 | A functional and folded helix shuffled domain B and its weak spot

We have been successful in creating helix-shuffled variants of domain B. These variants display the correct overall three-dimensional structure and possess Fc binding affinity, site, and selectivity as the wild type. Moreover, helices 2 and 3 are able to undergo the required conformational changes upon Fc binding. However, the thermodynamic stability is significantly reduced and the NMR structure identified the potential weak spot of the variant, a reduced length of helix 2 and a disordered loop 2, connecting helices 2 and 3. This might further affect the orientation of helix 3 and its packing to helices 1 and 2. It is likely that these local disruptions in the structure are causing at least some of the reduced thermodynamic stability. This structural weak spot is not involved in the binding site and therefore not affecting Fc binding. In other words, Fc binding and thermodynamic stability in the helix shuffled variant are decoupled and distributed to different structural areas. We only have selected for Fc binding, resulting in a folded binding site and high binding affinity and selectivity. We did not select for stability, resulting in a less folded area of the protein and much reduced thermodynamic stability. Because both aspects seem to be structurally separated, the thermodynamic stability could be reintroduced in future attempts without affecting binding. One Strategy to improve the thermal stability of the helix shuffle domain B is the introduction of single-point mutations. For domain B, such an engineering effort has already been demonstrated resulting in the more stable domain Z (Kanje et al., 2020). Moreover, loop grafting (Zhu et al., 2023) onto highly stable engineered protein A domains (Minakuchi et al., 2013) and the insertion of cysteines that form intramolecular disulfide bonds could stabilize the protein (Pikkemaat et al., 2002; Wiedemann et al., 2020). In addition, molecular dynamic simulation studies (Irumagawa et al., 2021) with a focus on loop 2 could be useful to target the weak spots responsible for thermal instability.

# 3 | MATERIALS AND METHODS

## 3.1 | Production of hIgG1-Fc and Avelumab-Fab

Mammalian expression of hIgG1-Fc and Avelumab-Fab was performed in Expi293F cells. Cells were cultured in shake flasks filled with Gibco Expi293 Expression medium (Fisher Scientific). On the day of transfection, cells were seeded with a density of 2.5 Mio/mL. For transfection, the Expi293 Transfection Kit (Thermo Fisher) was used according to the manufacturer's information. After 4 days, the supernatant was centrifuged and filtered. hIgG1-Fc was purified via a HiTrap Protein A HP column (Cytiva) according to the instructions of the manufacturer. hIgG1-Fc was purified via a HiTrap Protein A HP column (Cytiva) according to the instructions of the manufacturer. Avelumab-Fab was purified via a Capture Select IgG-CH1 column (Thermo) according to the manufacturer's instruction. For both hIgG1-Fc

1469896x, 2025, 2, Downloaded from https://onlinelibrary.wiley.com/doi/10.1002/pro.70012, Wiley Online Library on [22/01/2025]. See the Terms and Conditions (https://onlinelibrary.wiley.com/terms-and-conditions) on Wiley Online Library for rules of use; OA articles are governed by the applicable Creative Commons License

and Avelumab-Fab, a size exclusion chromatography via a HiLoad 26/600 Superdex 200 pg. column (Cytiva) in 1x PBS pH 7.3 was performed as the second purification step. Next, hIgG1-Fc and Avelumab-Fab were biotinylated using the EZ-Link Sulfo-NHS-LC-Biotinylation Kit from Thermo Scientific according to the manufacturer's instructions.

### 3.2 | Construction of domain B libraries

A gene fragment that encodes wt domain B (Uniprot ID P38507, sequence 212–269) was used as a template for the construction of cDNA libraries. Modular segments were defined at DNA level to connect the helices differently and insert two randomized loops (Figure 1). The loops are formed by three to five (loop 1) and six to eight (loop 2) randomized positions. The complete gene fragments were assembled using VNN oligonucleotides (Microsynth Seqlab) with degenerate bases (Virnekäs et al., 1994) (V = A, C, G; N = A, T, C, G) excluding codons for cysteine and aromatic amino acids. The modules were linked together using standard PCR techniques. Depending on the length and the combination of the two loops, 9–13 randomized positions were inserted resulting in a theoretical diversity of $10^{10}$–$10^{15}$ domain B variants at protein level.

### 3.3 | Selection and screening of domain B variants

The selection was performed by ribosome display (Amstutz et al., 2006) including the presentation of nascent domain B variants via ribosomal ternary complexes. 5′ regulatory sequences and a tolA-spacer region were fused to the DNA libraries via PCR to obtain functional constructs. The HiScribe T7 High Yield RNA Synthesis Kit (NEB) was used for in vitro transcription of RNA. In vitro translation was performed using the *E. coli* S30 Extract System for Linear Templates from Promega according to the manufacturer's instructions. To prevent dissociation of the noncovalently linked ternary complexes, the selection was performed at 15°C and in the presence of $Mg^{2+}$. In four rounds of biopanning, the ternary complexes were incubated with the biotinylated target protein hIgG1-Fc previously immobilized on streptavidin beads (Invitrogen). To increase selection pressure, the target concentration was reduced and the wash steps were successively extended in each round. IgG-binding ternary complexes were eluted from the beads by adding EDTA. The isolated mRNA was transcribed into cDNA followed by a final PCR to amplify the obtained pools for a new selection round. In round four, an off-rate selection was performed to obtain variants with high affinity. After binding of ternary complexes to 10 nM biotinylated hIgG1-Fc, a 1000-fold excess of non-biotinylated hIgG1-Fc was added to the mixture. At the end of the selection, the enriched binding molecules were cloned in an expression vector to obtain N-terminal fusions of domain B variants with GFP.

The screening of IgG-binding domain B variants was performed by ELISA. For hit screening, single colonies were picked and cultivated on a 384-well scale. After protein expression in BL21(DE3), cell lysis was performed via threefold freeze–thaw cycles. The supernatants were incubated with target protein hIgG1-Fc and off-target BSA coated on 384-well high-binding plates (Greiner). After plate washing, the fluorescence intensity of fused GFP at 483 nm excitation and 535 nm emission was measured using a microplate reader. Variants that showed high-affinity binding to hIgG1-Fc were selected as "hits" and produced on larger scale for further characterization.

### 3.4 | Purification of domain B variants

First, selected domain B variants were expressed as tag-free proteins in BL21(DE3). Protein expression was done on a 1-liter scale followed by cell harvest and lysis. For NMR spectroscopy, proteins were produced in M9 minimal medium (Miller, 1972) supplemented with $^{15}NH_4Cl$ and $^{13}C_6$-glucose, as the sole nitrogen and carbon sources. Second, tag-free domain B variants were purified via an IgG Sepharose 6 Fast Flow XK26/20 column (Cytiva) according to the instruction of the manufacturer. A size exclusion chromatography via a HiLoad 16/600 Superdex 75 pg. column (Cytiva) in 1x PBS pH 7.3 was performed as a second purification step.

### 3.5 | Surface plasmon resonance (SPR)

The binding of domain B variants to hIgG1-Fc and Avelumab-Fab was analyzed by surface plasmon resonance (SPR) (Liedberg et al., 1983; Turbadar, 1959) using a multichannel SPR-32 system (Bruker Daltonik) with corresponding CM5 sensor chips. hIgG1-Fc and Avelumab-Fab were immobilized on the chip surface by amine coupling through EDC/NHS followed by concentration-dependent injection of domain B variants (0–2000 nM) in 0.05% PBST pH 7.3. The samples were passed over the CM5 chip at a temperature of 20°C with a flow rate of 30 µL/min. After each cycle, the proteins on the surface of the chip were regenerated with 10 mM glycine pH 2.0. The obtained data were evaluated

1469896x, 2025, 2, Downloaded from https://onlinelibrary.wiley.com/doi/10.1002/pro.70012, Wiley Online Library on [22/01/2025]. See the Terms and Conditions (https://onlinelibrary.wiley.com/terms-and-conditions) on Wiley Online Library for rules of use; OA articles are governed by the applicable Creative Commons License

using the Sierra Analyzer software (Bruker Daltonik). $K_D$, $k_{on}$, and $k_{off}$ values were calculated by curve fitting using a global kinetic fitting model integrated into the software (1:1 Langmuir model).

## 3.6 | Circular dichroism (CD) and temperature-induced unfolding

Far-UV (200–250 nm) circular dichroism (CD) experiments on a Jasco J-810 spectropolarimeter were performed to analyze the secondary structure and thermal-induced structural transition of domain B variants. Proteins (0.2 mg/mL) diluted in 20 mM $NaH_2PO_4$ were transferred into a 1 mm quartz cuvette. The spectral measurements were performed in a temperature range of 10–90°C with a scanning rate of 50 nm/min at a bandwidth of 1 nm. An average of 16 spectra per sample was measured, and the baseline was corrected. Both the mean residual ellipticity and the proportion of α-helical secondary structure elements were calculated using the Spectra Manager I software according to the reference by Yang et al. (1986).

## 3.7 | Nuclear magnetic resonance (NMR) spectroscopy

All NMR experiments were performed on a Bruker Avance III 800 spectrometer equipped with a cryoprobe at 15°C. Unlabeled samples of wt domain B and the final construct at 0.5 mM concentration were used to initially evaluate the construct, although $^{15}N^{13}C$ samples of the construct at 1 mM concentration were used for assignment and structure calculation. Samples contain 137 mM NaCl, 2.7 mM KCl, 8 mM $Na_2HPO_4$, 2 mM $KH_2PO_4$, 10% D2O pH 6.5. An NMR titration experiment with hIgG1-Fc was performed by titrating Fc to $^{15}N^{13}C$ labeled protein (90 μM) to a final ratio of 1: 0.35. The titration was monitored by $^{1}H^{15}N$ HSQC experiments. Because the titration was in slow exchange on the NMR time scale peak volumes were determined and analyzed. Spectra were processed using NMRPipe (Delaglio et al., 1995) and analyzed using NMRView (Johnson, 2004). Resonances were assigned using HNCACB and HN(CO)CACB, H(C)CH-TOCSY as well as 3D TOCSY-HSQC experiments for $^{15}N$ nuclei and 3D NOESY-HSQC experiments for $^{15}N$ and $^{13}C$ aliphatic/aromatic nuclei. Structures were calculated using ARIA2.3 (Linge et al., 2003) with standard parameters with NOEs from the 3D NOESY-HSQC experiments, and Phi-Psi dihedral angle constraints were derived using TALOS (Shen et al., 2009). The lowest-energy models have been deposited in the PDB with accession number 9fzm.

## 3.8 | (GGIT/AKTNPGN) as affinity ligand for the purification of hIgG1

(GGIT/AKTNPGN) was immobilized at 10 mg/mL on 1 mL HiTrap NHS-Activated HP resin (Cytiva) according to the manufacturer's instructions. An ÄKTA system from Cytiva was used for all chromatography runs. All column experiments were performed at 10°C at a flow rate of 1 mL/min. The resin was equilibrated with 1x PBS pH 7.3 before 0.3 mg/mL of hIgG1 was injected into the column. After re-equilibration with 100 mM citrate, 150 mM NaCl pH 7.3, bound hIgG1 was eluted in a linear gradient with a constant slope between pH 7.3 and 3.0 over 15 column volumes. The UV absorbance at 280 nm was monitored to determine the pH at the elution peak maximum.

In this work, dynamic binding capacity (DBC) was measured and defined as the amount of hIgG1 loaded on the column before there is a 10% breakthrough of the protein. First, hIgG1 with a concentration of 1.5 mg/mL in 1x PBS pH 7.3 was flowed through the ÄKTA system in column bypass to determine the absorbance at 280 nm with 100% breakthrough. Next, hIgG1 was loaded onto the equilibrated column until 10% target breakthrough at 6 min residence time. The UV signal at 280 nm was monitored during the load phase to calculate DBC (Wang et al., 2024).

Further, chromatography runs with clarified Expi293-cell culture harvest spiked with hIgG1 (0.2 mg/mL) were performed. The column was equilibrated with 1x PBS pH 7.3, then loaded to 80% of the DBC determined from the DBC studies. Next, the column was washed with 20 column volumes 1x PBS pH 7.3 followed by an elution of hIgG1 with 100 mM citrate, 150 mM NaCl pH 4.8. Ten cycles of hIgG1 loading and elution were performed to investigate the column lifetime. Between each run, the column was stripped with 100 mM citrate pH 2.0.

## AUTHOR CONTRIBUTIONS

**Hanna Bobolowski:** Conceptualization; investigation; methodology; validation; formal analysis; writing – original draft. **Erik Fiedler:** Conceptualization; formal analysis; writing – original draft. **Ulrich Haupts:** Conceptualization. **Hauke Lilie:** Conceptualization; writing – original draft; formal analysis. **Ulrich Weininger:** Conceptualization; investigation; writing – original draft; formal analysis; validation.

## ACKNOWLEDGMENTS

We thank Jochen Balbach for free access to the NMR spectrometers. We also thank Manja Gloser-Bräunig and Anja Katzschmann for the production of Fc and Fab fragments. Open Access funding enabled and organized by Projekt DEAL.

1469896x, 2025, 2, Downloaded from https://onlinelibrary.wiley.com/doi/10.1002/pro.70012, Wiley Online Library on [22/01/2025]. See the Terms and Conditions (https://onlinelibrary.wiley.com/terms-and-conditions) on Wiley Online Library for rules of use; OA articles are governed by the applicable Creative Commons License

## ORCID

*Erik Fiedler* https://orcid.org/0000-0001-7345-5266
*Ulrich Haupts* https://orcid.org/0000-0003-0841-8332
*Hauke Lilie* https://orcid.org/0000-0003-1138-9448


## REFERENCES


Amstutz P, Binz HK, Zahnd C, Plückthun A. In: Celis JE, editor. Cell Biology. Burlington: Academic Press; 2006. p. 497–509.

Boehr DD, McElheny D, Dyson HJ, Wright PE. The dynamic energy landscape of dihydrofolate reductase catalysis. Science. 2006;313(5793):1638–42.

Choi YJ, Agarwal S, Deane CM. How long is a piece of loop? Peerj. 2013;1:e1.

Degrado WF, Wasserman ZR, Lear JD. Protein design, a minimalist approach. Science. 1989;243(4891):622–8.

Deis LN, Wu Q, Wang Y, Qi Y, Daniels KG, Zhou P, et al. Suppression of conformational heterogeneity at a protein-protein interface. Proc Natl Acad Sci U S A. 2015;112(29):9028–33.

Deisenhofer J. Crystallographic refinement and atomic models of a human fc fragment and its complex with fragment-B of protein-a from *Staphylococcus-aureus* at 2.9-a and 2.8-a resolution. Biochemistry. 1981;20(9):2361–70.

Delaglio F, Grzesiek S, Vuister GW, Zhu G, Pfeifer J, Bax A. Nmrpipe – a multidimensional spectral processing system based on Unix pipes. J Biomol NMR. 1995;6(3):277–93.

Dobbs AJ, Anderson BF, Faber HR, Baker EN. Three-dimensional structure of cytochrome c' from two Alcaligenes species and the implications for four-helix bundle structures. Acta Crystallogr D Biol Crystallogr. 1996;52(Pt 2):356–68.

Ey PL, Prowse SJ, Jenkin CR. Isolation of pure Igg1, Igg2a and Igg2b immunoglobulins from mouse serum using protein a-Sepharose. Immunochemistry. 1978;15(7):429–36.

Fersht A. Enzyme structure and mechanism. New York: W. H. Freeman; 1977.

Fiedler E, Katzschmann A, Boecker H, Meysing M, Lotze J, Bobolowski H. Specific baculovirus major envelope glycoprotein gp64 binding proteins (WO2023057617A1). Deutsches Patent- und Markenamt. https://depatisnet.dpma.de/DepatisNet/depatisnet?action=bibdat&docid=WO002023057617A1

Garg P. Selective preference of antibody mimetics over antibody, as binding molecules, for diagnostic and therapeutic applications in cancer therapy. Biointerface Res Appl Chem. 2021;11(3):10679–89.

Gebauer M, Skerra A. Engineered protein scaffolds as next-generation therapeutics. Annu Rev Pharmacol Toxicol. 2020;60(60):391–415.

Ghose S, Zhang J, Conley L, Caple R, Williams KP, Cecchini D. Maximizing binding capacity for protein A chromatography. Biotechnol Prog. 2014;30(6):1335–40.

Graille M, Stura EA, Corper AL, Sutton BJ, Taussig MJ, Charbonnier JB, et al. Crystal structure of a protein A domain complexed with the Fab fragment of a human IgM antibody:: structural basis for recognition of B-cell receptors and superantigen activity. Proc Natl Acad Sci USA. 2000;97(10):5399–404.

Gülich S, Uhlén M, Hober S. Protein engineering of an IgG-binding domain allows milder elution conditions during affinity chromatography. J Biotechnol. 2000;76(2–3):233–44.

Gunneriusson E, Nord K, Uhlén M, Nygren PÅ. Affinity maturation of a DNA polymerase specific affibody by helix shuffling. Protein Eng. 1999;12(10):873–8.

Huang PS, Oberdorfer G, Xu C, Pei XY, Nannenga BL, Rogers JM, et al. High thermodynamic stability of parametrically designed helical bundles. Science. 2014;346(6208):481–5.

Irumagawa S, Kobayashi K, Saito Y, Miyata T, Umetsu M, Kameda T, et al. Rational thermostabilisation of four-helix bundle dimeric de novo proteins. Sci Rep. 2021;11(1):7526.

Johnson BA. Using NMRView to visualize and analyze the NMR spectra of macromolecules. Methods Mol Biol. 2004;278:313–52.

Kahl M, Fiedler E, Bosse-Doenecke E et al., Binding protein specific for the spike protein of severe acute respiratory syndrome corona virus 2 (sars-cov-2) (WO2021260075A1). Deutsches Patent- und Markenamt. https://depatisnet.dpma.de/DepatisNet/depatisnet?action=bibdat&docid=WO002021260075A1

Kanje S, Scheffel J, Nilvebrant J, Hober S. Chapter 2 – engineering of protein a for improved purification of antibodies and Fc-fused proteins. In: Matte A, editor. Approaches to the purification, analysis and characterization of antibody-based therapeutics. Amsterdam: Elsevier; 2020. p. 35–54.

Kikuchi Y, Uno S, Nanami M, Yoshimura Y, Iida SI, Fukushima N, et al. Determination of concentration and binding affinity of antibody fragments by use of surface plasmon resonance. J Biosci Bioeng. 2005;100(3):311–7.

Köhler C, Carlström G, Gunnarsson A, Weininger U, Tångefjord S, Ullah V, et al. Dynamic allosteric communication pathway directing differential activation of the glucocorticoid receptor. Sci Adv. 2020;6(29):eabb5277.

Krepper W, Satzer P, Beyer BM, Jungbauer A. Temperature dependence of antibody adsorption in protein A affinity chromatography. J Chromatogr A. 2018;1551:59–68.

Kresse HP, Czubayko M, Nyakatura G, Vriend G, Sander C, Bloecker H. Four-helix bundle topology re-engineered: monomeric Rop protein variants with different loop arrangements. Protein Eng. 2001;14(11):897–901.

Krieger F, Möglich A, Kiefhaber T. Effect of proline and glycine residues on dynamics and barriers of loop formation in polypeptide chains. J Am Chem Soc. 2005;127(10):3346–52.

Liedberg B, Nylander C, Lundstrom I. Surface-plasmon resonance for gas-detection and biosensing. Sensors Actuators. 1983;4(2):299–304.

Linge JP, Habeck M, Rieping W, Nilges M. ARIA: automated NOE assignment and NMR structure calculation. Bioinformatics. 2003;19(2):315–6.

Linhult M, Gülich S, Gräslund T, Simon A, Karlsson M, Sjöberg A, et al. Improving the tolerance of a protein a analogue to repeated alkaline exposures using a bypass mutagenesis approach. Proteins-Structure Func Bioinform. 2004;55(2):407–16.

Litwack G. Human biochemistry. Amsterdam: Elsevier Science; 2017.

Miller JH. Experiments in molecular genetics. New York: Cold Spring Harbor Laboratory; 1972.

Minakuchi K, Murata D, Okubo Y, Nakano Y, Yoshida S. Remarkable alkaline stability of an engineered protein A as immunoglobulin affinity ligand: C domain having only one amino acid substitution. Protein Sci. 2013;22(9):1230–8.


1469896x, 2025, 2, Downloaded from https://onlinelibrary.wiley.com/doi/10.1002/pro.70012, Wiley Online Library on [22/01/2025]. See the Terms and Conditions (https://onlinelibrary.wiley.com/terms-and-conditions) on Wiley Online Library for rules of use; OA articles are governed by the applicable Creative Commons License

Mouratou B, Behar G, Pecorari F. Artificial affinity proteins as ligands of immunoglobulins. Biomolecules. 2015;5(1):60–75.
Myers JK, Oas TG. Preorganized secondary structure as an important determinant of fast protein folding. Nat Struct Biol. 2001; 8(6):552–8.
Nilvebrant J, Hober S. The albumin-binding domain as a scaffold for protein engineering. Computational and structural Biotechnol J. 2013;6:e201303009.
Pershad K, Kay BK. Generating thermal stable variants of protein domains through phage display. Methods. 2013;60(1):38–45.
Pikkemaat MG, Linssen ABM, Berendsen HJC, Janssen DB. Molecular dynamics simulations as a tool for improving protein stability. Protein Eng. 2002;15(3):185–92.
Predki PF, Regan L. Redesigning the topology of a 4-helix-bundle protein – monomeric Rop. Biochemistry. 1995;34(31):9834–9.
Richardson JS, Richardson DC. Amino-acid preferences for specific locations at the ends of alpha-helices. Science. 1988;240(4859): 1648–52.
Rigi G, Ghaedmohammadi S, Ahmadian G. A comprehensive review on staphylococcal protein a (SpA): its production and applications. Biotechnol Appl Biochem. 2019;66(3):454–64.
Scheffel J, Kanje S, Borin J, Hober S. Optimization of a calcium-dependent protein A-derived domain for mild antibody purification. MAbs. 2019;11(8):1492–501.
Shao Q, Gao YQ. The relative helix and hydrogen bond stability in the B domain of protein A as revealed by integrated tempering sampling molecular dynamics simulation. J Chem Phys. 2011; 135(13):102–112.
Shen Y, Delaglio F, Cornilescu G, Bax A. TALOS plus: a hybrid method for predicting protein backbone torsion angles from NMR chemical shifts. J Biomol NMR. 2009;44(4):213–23.
Shoemaker KR, Kim PS, Brems DN, Marqusee S, York EJ, Chaiken IM, et al. Nature of the charged-group effect on the stability of the C-peptide helix. Proc Natl Acad Sci USA. 1985; 82(8):2349–53.
Ståhl S, Gräslund T, Eriksson Karlström A, Frejd FY, Nygren PÅ, Löfblom J. Affibody molecules in biotechnological and medical applications. Trends Biotechnol. 2017;35(8):691–712.
Starovasnik MA, Braisted AC, Wells JA. Structural mimicry of a native protein by a minimized binding domain. Proc Natl Acad Sci USA. 1997;94(19):10080–5.
Tobi D, Bahar I. Structural changes involved in protein binding correlate with intrinsic motions of proteins in the unbound state. Proc Natl Acad Sci USA. 2005;102(52):18908–13.
Tsukamoto M, Watanabe H, Ooishi A, Honda S. Engineered protein a ligands, derived from a histidine-scanning library, facilitate the affinity purification of IgG under mild acidic conditions. J Biol Eng. 2014;8:15–23.
Turbadar T. Complete absorption of light by thin metal films. Proc Phys Soc London. 1959;73(469):40–4.
van Rosmalen M, Krom M, Merkx M. Tuning the flexibility of glycine-serine linkers to allow rational design of multidomain proteins. Biochemistry. 2017;56(50):6565–74.
Virnekäs B, Ge L, Plückthun A, Schneider KC, Wellnhofer G, Moroney SE. Trinucleotide phosphoramidites – ideal reagents for the synthesis of mixed oligonucleotides for random mutagenesis. Nucleic Acids Res. 1994;22(25):5600–7.
Wang FAS, Fan Y, Chung WK, Dutta A, Fiedler E, Haupts U, et al. Evaluation of mild pH elution protein a resins for antibodies and fc-fusion proteins. J Chromatogr A. 2024;1713:464523.
Wang H, Liu R. Advantages of mRNA display selections over other selection techniques for investigation of protein–protein interactions. Expert Rev Proteomics. 2011;8(3):335–46.
Wiedemann C, Kumar A, Lang A, Ohlenschläger O. Cysteines and disulfide bonds as structure-forming units: insights from different domains of life and the potential for characterization by NMR. Front Chem. 2020;8:820.
Worth CL, Blundell TL. On the evolutionary conservation of hydrogen bonds made by buried polar amino acids: the hidden joists, braces and trusses of protein architecture. BMC Evol Biol. 2010;161:10.
Yang JT, Wu CSC, Martinez HM. Methods in enzymology. Cambridge: Academic Press; 1986. p. 208–69.
Zhu MY, Zhai W, Jiang H, Lin L, Wei W, Wei D. Exploiting loop-grafting strategy resorting on computer-aided design to improve the thermostability of alpha-amylase from *Geobacillus stearothermophilus*. Process Biochem. 2023;133:28–38.

## SUPPORTING INFORMATION

Additional supporting information can be found online in the Supporting Information section at the end of this article.

**How to cite this article:** Bobolowski H, Fiedler E, Haupts U, Lilie H, Weininger U. A functional helix shuffled variant of the B domain of *Staphylococcus aureus*. Protein Science. 2025;34(2): e70012. https://doi.org/10.1002/pro.70012

1469896x, 2025, 2, Downloaded from https://onlinelibrary.wiley.com/doi/10.1002/pro.70012, Wiley Online Library on [22/01/2025]. See the Terms and Conditions (https://onlinelibrary.wiley.com/terms-and-conditions) on Wiley Online Library for rules of use; OA articles are governed by the applicable Creative Commons License